J Biomol NMR (2014) 60:1–9
DOI 10.1007/s10858-014-9847-x

COMMUNICATION

HNCA+, HNCO+, and HNCACB+ experiments: improved performance by simultaneous detection of orthogonal coherence transfer pathways

Sergio Gil-Caballero · Adrien Favier · Bernhard Brutscher

Received: 13 May 2014 / Accepted: 7 July 2014 / Published online: 24 July 2014

Abstract Three experiments, BEST–TROSY HNCA+, HNCO+ and HNCACB+ are presented for sequential backbone resonance assignment of ^{13}C, ^{15}N labelled proteins. The novelty of these experiments with respect to conventional pulse sequences is the detection of additional orthogonal coherence transfer pathways that results in enhanced sensitivity for sequential correlations without significantly compromising the intensity of intra-residue correlation peaks. In addition, a 2-step phase cycle separates peaks originating from the orthogonal coherence transfer pathways in 2 sub-spectra, thus providing similar information as obtained from performing a pair of sequential and intra-residue correlation experiments.

Keywords Assignment · Protein · BEST · TROSY · Sensitivity · Time-shared data acquisition

Electronic supplementary material The online version of this article (doi:10.1007/s10858-014-9847-x) contains supplementary material, which is available to authorized users.

S. Gil-Caballero · A. Favier · B. Brutscher (✉)
Institut de Biologie Structurale, Université Grenoble 1, 71 Avenue des Martyrs, 38044 Grenoble Cedex 9, France
e-mail: bernhard.brutscher@ibs.fr

S. Gil-Caballero · A. Favier · B. Brutscher
Commissariat à l'Energie Atomique et aux Energies Alternatives (CEA), Grenoble, France

S. Gil-Caballero · A. Favier · B. Brutscher
Centre National de Recherche Scientifique (CNRS), Grenoble, France

Introduction

Sequential resonance assignment of ^{13}C,^{15}N labeled proteins is usually achieved by a combination of 3D or higher-dimensional HNC-type correlation experiments providing complementary information about sequentially adjacent amide groups (Ikura et al. 1990; Sattler et al. 1999), complemented by some additional amino-acid-type information. A first class of experiments, HNCA, HNCACB, and HNCACO, exploits the N-CA coupling for coherence transfer. In these *bi-directional* experiments, both intra-residue (N_i–CA_i) as well as sequential (N_i–CA_{i-1}) correlation peaks are detected due to a similar size of the $^1J_{NC}\alpha$ and $^2J_{NC}\alpha$ coupling constants. For unambiguous identification of sequential correlation peaks, purely *sequential* HNCO, HNCOCA and HNCOCACB experiments can be recorded, where ^{15}N coherence is transferred in a relay step via ^{13}CO to ^{13}CA, thus relying only on unambiguous one-bond scalar couplings, $^1J_{NCO}$ and $^1J_{COC}\alpha$. Alternatively, intra-residue iHNCA and iHNCACB experiments (Brutscher 2002; Nietlispach et al. 2002; Permi 2002) have been proposed that suppress to a large extent the sequential coherence transfer pathway, thus resulting in pure intra-residue correlation spectra.

Here we present a set of new experiments, HNCA+, HNCACB+, and HNCO+ that result in spectra similar to standard HNCA, HNCACB and HN(CA)CO, but with the particularity that all 4 (instead of only 2) coherence transfer pathways created by a N–CA transfer step contribute to the detected signal. This results in an important signal improvement for the sequential correlation peaks at the expense of some signal loss for the intra-residue peaks. In addition, a simple 2-step IPAP-type (Ottiger et al. 1998) phase-cycle scheme allows separating orthogonal coherence transfer pathways for the discrimination between

sequential and intra-residue correlations. These experiments are thus conceptually similar to so-called *time-shared* techniques where 2 complementary correlation spectra are acquired simultaneously by the same pulse sequence either during a single detection period (Boelens et al. 1994; Frueh et al. 2005; Guo et al. 2008), or by using sequential data acquisition with or without dual receivers (Chakraborty et al. 2012; Haasnoot et al. 1984; Kupče and Kay 2012; Kupče et al. 2010; Wiedemann et al. 2014). We would like to mention that a different HNCA(+) experiment has already been proposed in the past by the Wider group (Salzmann et al. 2000) that is conceptually different from the experiments proposed here. In the Wider experiment, 2 coherence transfer pathways starting from H^{α} and H^{N} polarization, respectively, are detected in a single acquisition period to increase the experimental sensitivity. We demonstrate the performance of our new pulse schemes for different protein samples: the small 8 kDa protein ubiquitin, a 30 kDa complex of the dimeric bleomycin-resistance protein (BRP) and bleomycin, and an intrinsically disordered C-terminal 257-residue fragment of the HCV protein NS5A.

The pulse sequences for the HNCA+, HNCACB+, and HNCO+ experiments are conceptually derived by inserting additional coherence transfer blocks (Fig. 1d) into conventional HNCA (Fig. 1a), HN(CA)CO (Fig. 1b), and HNCACB (Fig. 1c) sequences, and by insuring correct refocusing of ^{15}N coherence present during these additional transfer delays and the t_1 frequency editing period (see below). The experiments, shown in Fig. 1, have been implemented as BEST-TROSY (BT) versions (Farjon et al. 2009; Favier and Brutscher 2011; Solyom et al. 2013) to improve the overall sensitivity, and reduce experimental time requirements. The basic features of these new experiments, however, are independent of the BEST–TROSY scheme, and can be easily transferred to standard HSQC- or TROSY-type implementations of these experiments.

All experiments are of the out-and back transfer type, starting from amide ^{1}H (and ^{15}N in the case of BEST–TROSY) polarization. After the initial ^{1}H–^{15}N INEPT step, the four relevant coherence transfer pathways (CTP) for the HNCA+ experiment ("out" pathway) are as follows:

$$N_x^i \xrightarrow{2\Delta_1\left({}^1J_{NC\alpha},{}^2J_{NC\alpha}\right)} 2N_y^iCA_z^i \xrightarrow{90N} 2N_z^iCA_z^i \xrightarrow{2\Delta_2\left({}^1J_{NCo}\right)} 2N_z^iCA_z^i \xrightarrow{2\Delta_3\left({}^1J_{COC\alpha}\right)} 2N_z^iCA_x^i \xrightarrow{t_1(CA)} \ldots \quad \text{(I - intra)} \tag{1}$$

$$N_x^i \xrightarrow{2\Delta_1\left({}^1J_{NC\alpha},{}^2J_{NC\alpha}\right)} 2N_y^iCA_z^{i-1} \xrightarrow{90N} 2N_z^iCA_z^{i-1} \xrightarrow{2\Delta_2\left({}^1J_{NCO}\right)} 2N_z^iCA_z^{i-1} \xrightarrow{2\Delta_3\left({}^1J_{COC\alpha}\right)} 2N_z^iCA_x^{i-1} \xrightarrow{t_1(CA)} \ldots \quad \text{(I - seq)} \tag{2}$$

Fig. 1 Pulse sequences of BEST–TROSY-type HNCA+ (**a** + **d**), HNCO+ (**b** + **d**), and HNCACB+ (**c** + **d**) experiments. Filled and open pulse symbols indicate 90° and 180° rf pulses, respectively. Unless indicated, all pulses are applied with phase x. The following pulse shapes are used for selective ^{1}H and ^{13}C pulses: (1) PC9 (Kupce and Freeman 1994), (2) REBURP, (3) E-BURP2, (4) double-band (db) REBURP (Geen and Freeman 1991), and (5) I-SNOB2 (Kupce et al. 1995). A *star* indicates a flip-back pulse obtained by time inversion of the excitation pulse shape. Open squares on ^{1}H indicate BIP-720-50-20 broadband inversion pulses (Smith et al. 2001). BIP ^{1}H pulses are always applied as pairs for ^{1}H–^{15}N recoupling or ^{1}H–^{13}C decoupling purposes, resulting in a 360° rotation on ^{1}H polarization. Selective amide ^{1}H pulses are typically centred at 8.5 ppm, covering a bandwidth of 4.0 ppm. ^{13}CO (^{13}CA, ^{13}CACB) EBURP, REBURP, and I-SNOB2 pulses are centred at 175 ppm (54 ppm, 35 ppm) covering a bandwidth of 80 ppm (100 ppm for PC9). The db-REBURP pulses cover a bandwidth of 35 ppm for the CO → CA transfer, and 24 ppm for the CA → CO transfer. The transfer delays common to BEST–TROSY sequences are adjusted to $\tau = 1/(4J_{NH}) - 0.5\delta_1 - 0.5\delta_2$, $\tau_1 = 1/(4J_{NH})$, $\tau_2 = 1/(4J_{NH}) - 0.5\delta_3 - 0.5\delta_2$, $\tau_3 = 1/(4J_{NH}) - 0.5\delta_2$, $\Delta_1 \approx 1/(4J_{NC\alpha})$, $\Delta_2 = 1/(4J_{NCO})$, $\Delta_3 = 1/(4J_{COC\alpha})$, $\Delta_4 = 1/(8J_{C\alpha C\beta})$, $t2a = \Delta_1 - t_2/2 + t2b$, and $t2b = 0$, with $1/(4J_{NH}) \approx 2.7$ ms, $1/(4J_{NC\alpha}) \approx 11$ ms, $1/(4J_{NCO}) \approx 15$ ms, $1/(4J_{COC\alpha}) \approx 4.5$ ms, and $1/(8J_{C\alpha C\beta}) \approx 3.7$ ms (for detection of both CA and CB correlations). The delays δ_1, δ_2 and δ_3 correspond to the ^{1}H pulse lengths of the PC9, REBURP and E-BURP2, respectively. In (**c**) the delay δ corresponds to the ^{13}C REBURP pulse length. For semi-CT ^{15}N editing, the delay t2b is incremented together with t_2 using the following time increment: $\Delta t_2 = (t_2^{max}/2 - \Delta_1)/N_2$ with N_2 the number of total increments in the t_2 dimension. Pulse field gradients G1-G8 are applied along the z-axis (PFGz) with durations of 300 to 500 µs and field strengths ranging from 6 to 43 G/cm. The 2-step phase cycle is: $\phi_1 = x; \phi_2 = x, -x; \phi_3 = x$ for in-phase (IP) spectrum, $\phi_3 = x$ for anti-phase (AP) spectrum; $\phi_4 = x; \phi_5 = y; \phi_6 = y, \phi_7 = x; \phi_8 = y,-y; \phi_{rec} = x, -x$. Addition and subtraction of IP and AP data sets allows selecting CTP-I and CTP-II, respectively. Quadrature detection in t_1 is obtained by time-proportional phase incrementation of ϕ_2 (and ϕ_8 in the case of HNCACB+) according to States-TPPI. For quadrature detection in t_2, data are recorded by selecting G4, G6 and G8 according to (−8:2:3.013) and (−7:3:1.987) for echo and antiecho, respectively, together with a 180° phase increment of ϕ_5 and ϕ_6. In order to avoid significant first order phase corrections in the ^{13}C dimension of the HNCA+ and HNCO+ experiments, the 180° ^{13}C and ^{1}H decoupling pulses are omitted for the first t_1 increments, and a Bloch-Siegert phase correction (∼140°) is applied to the pulse phases ϕ_2, ϕ_7, and ϕ_8. Pulse sequence codes for Bruker spectrometers are provided in the Supporting Information. The sequences and Python setup scripts are also directly available from the authors upon request

$$N_x^i \xrightarrow{2\Delta_1\left({}^1J_{NC\alpha},{}^2J_{NC\alpha}\right)} 4N_x^iCA_z^iCA_z^{i-1} \xrightarrow{90N} 4N_x^iCA_z^iCA_z^{i-1} \xrightarrow{2\Delta_2\left({}^1J_{NCo}\right)} 8N_y^iCO_z^{i-1}CA_z^iCA_z^{i-1} \xrightarrow{90CO} 8N_y^iCO_y^{i-1}CA_z^iCA_z^{i-1} \xrightarrow{2\Delta_3\left({}^1J_{COC\alpha}\right)} 4N_y^iCO_z^{i-1}CA_x^{i-1} \xrightarrow{t_1(CA)} \ldots \quad \text{(II - intra)} \tag{3}$$

$$N_x^i \xrightarrow{2\Delta_1\left({}^1J_{NC\alpha},{}^2J_{NC\alpha}\right)} N_x^i \xrightarrow{90N} N_x^i \xrightarrow{2\Delta_2\left({}^1J_{NCo}\right)} 2N_y^iCO_z^{i-1} \xrightarrow{90CO} 4N_y^iCO_y^{i-1} \xrightarrow{2\Delta_3\left({}^1J_{COC\alpha}\right)} 4N_y^iCO_z^{i-1}CA_x^{i-1} \xrightarrow{t_1(CA)} \ldots \quad \text{(II - seq)} \tag{4}$$

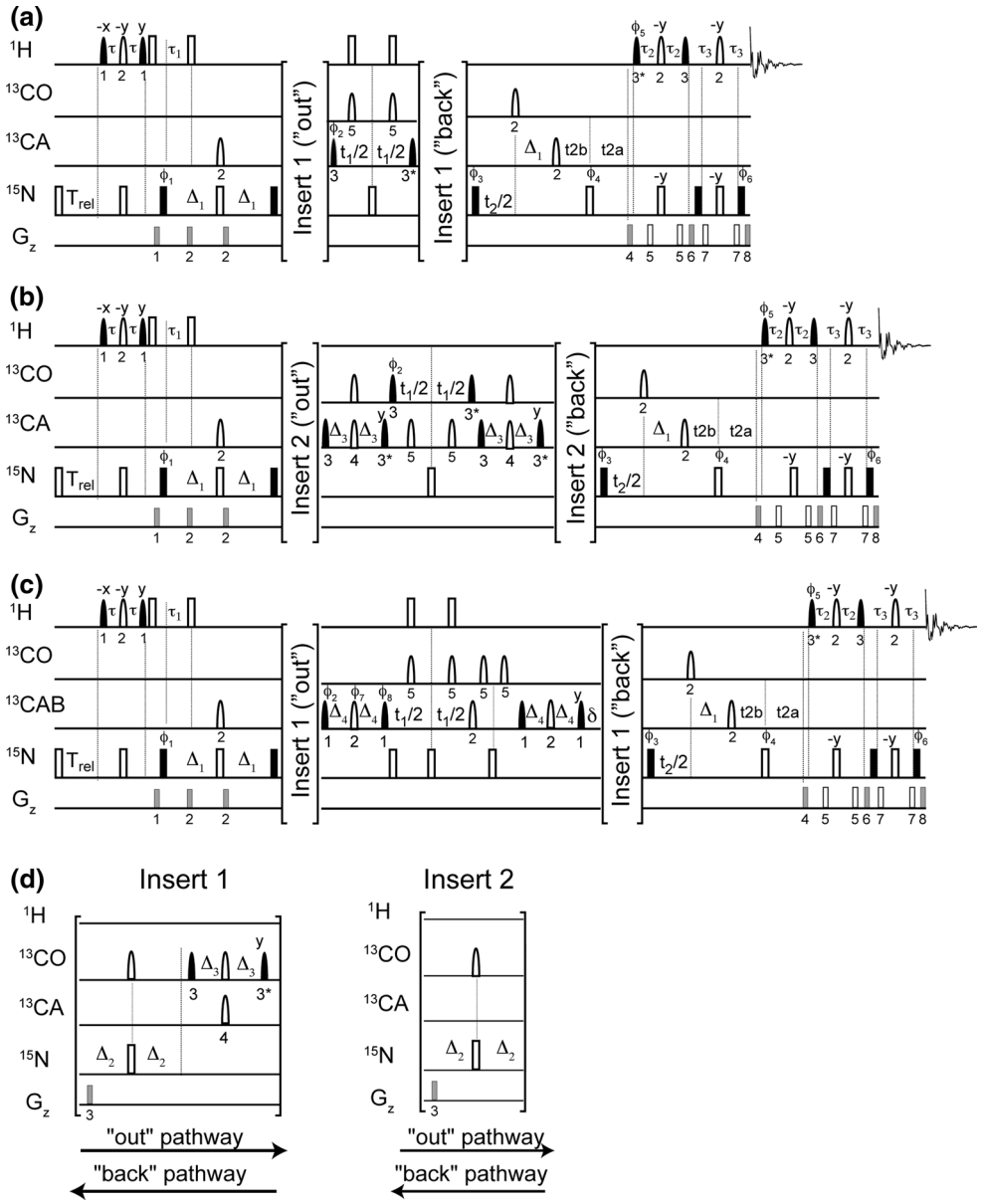

We can distinguish between 2 main pathways (I and II) that are orthogonal with respect to the ^{15}N spin state (coherence) after the N → CA transfer step of duration $2\Delta_1$. Both pathways give rise to a sequential (N_i–CA_{i-1}) and an intra-residue (N_i-CA_i) correlation peak. In a standard HNCA experiment, only CTP I results in detected NMR signal, while in the HNCA+ pulse scheme the additional pathways II are recovered (and detected) by additional transfer steps, N → CO → CA. The transfer amplitudes (TA) for the individual pathways (neglecting spin relaxation) are given by:

$$
\begin{aligned}
TA(I-\mathrm{intra}) &= \left(\sin\left(\pi^1 J_{NC\alpha} 2\Delta_1\right)\cos\left(\pi^2 J_{NC\alpha} 2\Delta_1\right)\right)^2 \\
TA(I-seq) &= \left(\cos\left(\pi^1 J_{NC\alpha} 2\Delta_1\right)\sin\left(\pi^2 J_{NC\alpha} 2\Delta_1\right)\right)^2 \\
TA(II-\mathrm{intra}) &= \left(\sin\left(\pi^1 J_{NC\alpha} 2\Delta_1\right)\sin\left(\pi^2 J_{NC\alpha} 2\Delta_1\right)\right. \\
&\quad \left.\times \sin\left(\pi^1 J_{NCO} 2\Delta_2\right)\sin\left(\pi^1 J_{COC\alpha} 2\Delta_3\right)\right)^2 \\
TA(II-seq) &= \left(\cos\left(\pi^1 J_{NC\alpha} 2\Delta_1\right)\right. \\
&\quad \left.\times \cos\left(\pi^2 J_{NC\alpha} 2\Delta_1\right)\sin\left(\pi^1 J_{NCO} 2\Delta_2\right)\sin\left(\pi^1 J_{COC\alpha} 2\Delta_3\right)\right)^2
\end{aligned}
\tag{5}
$$

The square takes into account that each transfer takes place twice for "out" and "back" transfers. For optimal

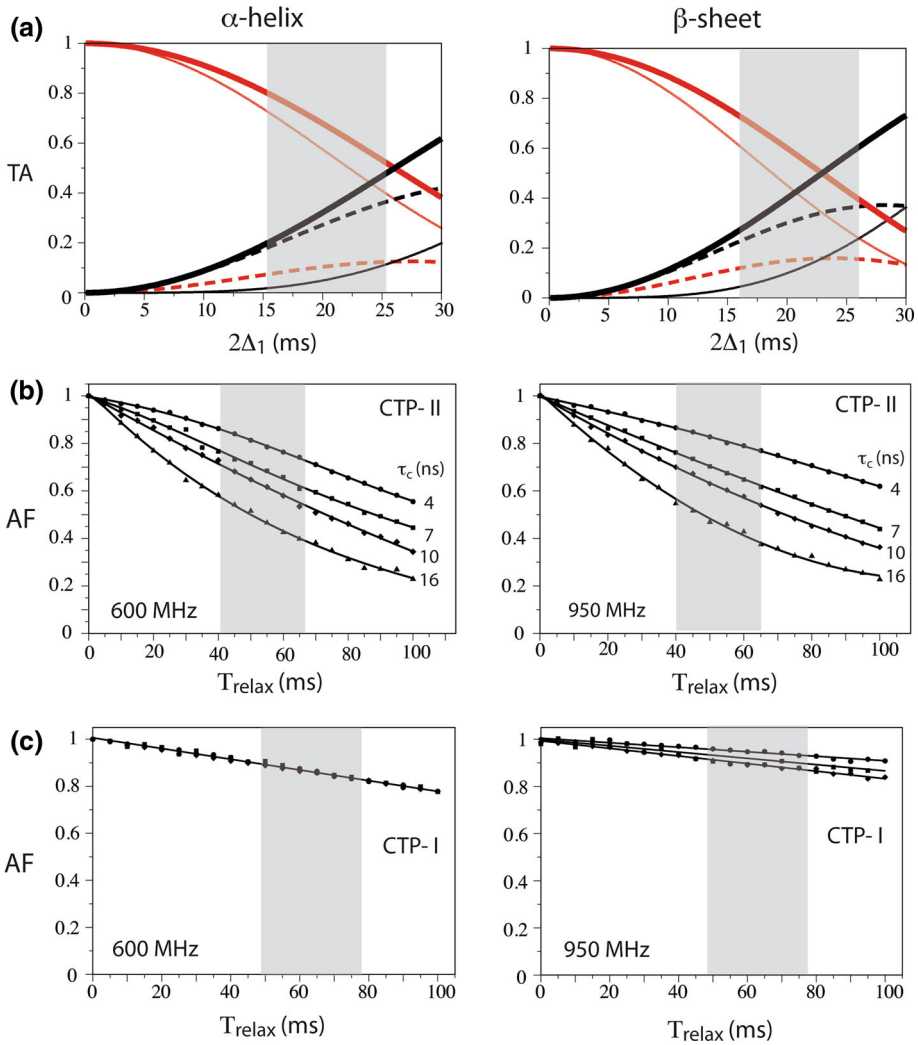

Fig. 2 Theoretical and experimental characterization of transfer efficiencies in HNCX+ experiments. **a** Transfer amplitudes (TA) calculated according to Eq. (5) as a function of the transfer delay $2\Delta_1$ for average scalar couplings in α-helical ($^1J_{NC\alpha} = 9.6$ Hz, $^2J_{NC\alpha} = 6.4$ Hz) and β-sheet ($^1J_{NC\alpha} = 10.9$ Hz, $^2J_{NC\alpha} = 8.3$ Hz) conformations (Delaglio et al. 1991). The terms $\sin(\pi^1 J_{COC\alpha} 2\Delta_3)$ and $\sin(\pi^1 J_{CO\alpha} 2\Delta_3)$ have been set to 1 for this calculation. Red and black lines correspond to transfer pathways giving rise to sequential and intra-residue correlation peaks, respectively. The transfer amplitudes for CTP-I are indicated by dashed lines, while those of CTP-II are shown as thin straight lines. In addition, the sum of the 2 CTP for either sequential and intra-residue correlations is shown as thick lines. The relaxation-induced signal loss during a relaxation delay T_{relax}, are shown in (**b**) and (**c**). Data have been measured at 2 different magnetic field strengths, 600 MHz (*left panels*), and 950 MHz ^{1}H frequency (*right panels*), and for different (estimated) molecular tumbling correlation times, 4 ns (*circles*), 7 ns (*squares*), 10 ns (*lozenges*), and 16 ns (*triangles*). The measured data points correspond to integrated 1D spectra recorded with the pulse sequence of Fig. 1a, replacing the inserts and t_1 editing blocks by a relaxation delay. The recycle delay was set to $T_{rec} = 200$ ms. Separation of the two CTP (I and II) has been achieved by phase cycling as explained in the text. The data shown in **b** provide an estimate of the relaxation induced signal loss for the CTP-II pathway with respect to the corresponding sequential correlation experiment, with the relevant relaxation time $T_{relax} = 4(\Delta_1 + \Delta_3) = 54$–$66$ ms for HNCA+ and HNCACB+, and $T_{relax} = 4\Delta_1 = 40$–$48$ ms for HNCO+. Similarly, the data in **c** provide an estimate of the relaxation induced signal loss for the CTP-I pathway with respect to the corresponding bi-directional correlation experiment, with the relevant relaxation time $T_{relax} = 4(\Delta_2 + \Delta_3) = 62$–$78$ ms for HNCA+ and HNCACB+, and $T_{relax} = 4\Delta_2 = 48$–$60$ ms for HNCO+

sensitivity of the experiment the transfer delays Δ_2 and Δ_3 should be set close to $\Delta_2 = 1/(4J_{NCO}) \approx 15$ ms and $\Delta_3 = 1/(4J_{COC\alpha}) \approx 4.5$ ms. As usual, these delays can be freely adjusted to account for spin-relaxation induced signal loss during the individual transfer steps. The transfer amplitudes computed for $^1J_{NC\alpha}$ and $^2J_{NC\alpha}$ coupling constants, characteristic of α-helical and β-sheet conformation in proteins (Delaglio et al. 1991) are plotted in Fig. 2a as a function of the transfer delay $2\Delta_1$. In the absence of significant spin relaxation, the sum of the 4 transfer amplitudes equals 1, and the choice of the transfer delay Δ_1 allows to adjust the relative intensity of intra-

residue and sequential correlation peaks. In particular this makes it possible to record HNCA correlation spectra where both, intra-residue and sequential peaks, have similar intensity as will be experimentally demonstrated below. The corresponding CTPs and transfer amplitudes for the HNCACB+ and HNCO+ experiments are provided in the Supporting Information.

After the initial N → CA transfer step, the ^{15}N spin state remains orthogonal for the 2 coherence-transfer pathways, CTP-I and CTP-II. While CTP-I evolves as longitudinal 2-spin order $2N_zCA_z$ [Eqs. (1) and (2)], thus limiting relaxation-induced signal loss for this pathway that corresponds to the signal detected in a standard HNCA experiment, the relevant spin density operators for CTP-II contain additional ^{15}N transverse components N_x or N_y. [Eqs. (3) and (4)]. To simplify the discussion, we have neglected here that in a TROSY-type implementation the ^{15}N spin state is a combination of N_z (N_x) and $2N_zH_z$ ($2N_xH_z$). In order to estimate experimentally the additional relaxation-induced signal loss in HNCX+ experiments with respect to bi-directional HNCX (for CTP-I) and sequential HNCOCX (for CTP–II), we have performed relaxation measurements. We have replaced the inserts (and the t_1 editing block) of Fig. 1a by a simple (chemical shift refocused) delay T_{relax}, and we have recorded 1D spectra as a function of this relaxation time, representative of the additionally required transfer or spin evolution delays in HNCX+. Phase cycling was used, as explained in the caption of Fig. 1, to select either CTP-I or CTP-II pathways. Data were recorded on 2 protein samples: (i) 2 mM [U–^{13}C, U–^{15}N]-labelled ubiquitin (76 residues) in 20 mM Hepes buffer at pH 6.1; and (ii) 1 mM [U–^{13}C, U–^{15}N]-labelled bleomycine-resistance protein, BRP (2 × 124 residues) in complex with Zn^{2+}-bound bleomycine (Vanbelle et al. 2003) in 20 mM MES buffer, 100 mM NaCl, 0.05 % NaN at pH 6.45. In order to obtain experimental data for different tumbling correlation times (τ_c), the experiments were repeated for ubiquitin at 25 °C ($\tau_c \approx 4$ ns) and 5 °C ($\tau_c \approx 7$ ns), as well as for BRP at 40 °C ($\tau_c \approx 10$ ns) and 20 °C ($\tau_c \approx 16$ ns). The results obtained at magnetic field strengths of 600 MHz (14.1 T) and 950 MHz (22.3 T) are shown in Fig. 2b for CTP-II and in Fig. 2c for CTP-I. As expected, the signal loss for CTP-II augments with increasing tumbling correlation time, and is slightly attenuated at higher field strengths (Fig. 2b). Compared to a standard sequential correlation experiment, the additional relaxation occurs during $T_{relax} = 4(\Delta_1 + \Delta_3)$ in HNCA+ and HNCACB+, or $4\Delta_1$ in HNCO+. For typical transfer delays ($T_{relax} = 40$–66 ms) the attenuation factor varies from about 0.8 for a small protein ($\tau_c \approx 4$ ns) at 950 MHz to 0.4 for a larger protein ($\tau_c \approx 16$ ns) at 600 MHz. Relaxation-induced signal loss for this pathway is limited by the BEST-TROSY implementation: CSA-DD cross-correlation (Pervushin et al. 1998) combined with ^{15}N polarization enhancement under fast-pulsing conditions (Favier and Brutscher 2011) yields longer apparent T_2 relaxation times compared to standard HSQC-based implementations. The data shown in Fig. 2c provide a measure of the relaxation–induced signal loss for CTP-I compared to a standard bi-directional experiment, during the additional transfer delay $T_{relax} = 4(\Delta_2 + \Delta_3)$ in HNCA+ and HNCACB+, or $4\Delta_2$ in HNCO+. For typical transfer delays ($T_{relax} = 48$–78 - ms), the attenuation factor is higher than 0.8, independent of the protein's tumbling correlation time and the magnetic field strength (within the studied range). These results indicate that the enhanced pulse schemes proposed here should be advantageously applicable to a wide range of small to medium-sized proteins.

In order to further evaluate the performance of these new experiments we have recorded 2D ^{1}H-^{13}C data sets of BT-HNCA+, BT-HNCO+, and BT-HNCACB+ for different N–CA transfer delays Δ_1, and compared them to the corresponding conventional BEST–TROSY sequences, lacking the additional transfer blocks (pulse sequences of Fig. 1a, b, and c without Inserts). Representative spectral regions of the data sets recorded for ubiquitin at 25 °C and 600 MHz are plotted in Fig. 3 (HNCA), and in the Supporting Information figures S1 (HNCO) and S2 (HNCACB). For the enhanced (+) pulse schemes, 2 data sets were recorded with the ^{15}N 90° pulse phase ϕ_3 either set to +x or −x. This phase change inverts the relative sign of peaks arising from CTPs I and II. As a result, in the first spectrum, all peaks have the same sign, while in the second spectrum peaks from different pathways have opposite sign. Therefore, addition and subtraction of the 2 spectra leads to the separation of signals originating from CTP-I and CTP-II. These sub-spectra provide information, very similar to a pair of HNCA and HN(CO)CA, typically used to distinguish sequential from intra-residue correlation peaks. The only difference here is that in the CTP-I spectrum also intra-residue peaks are detected, but with much lower intensity compared to the sequential ones. In the following, we will thus refer to this sub-spectrum as HN(CO)CA-like. Histograms (average and standard deviation) of intra-residue and sequential correlation peak intensities measured in these spectra with $\Delta_1 = 20$ ms are plotted in Fig. 3a. The same experiments and data analysis were also performed on BRP at 40 °C and 850 MHz, and the resulting histograms are shown in Fig. 4b. For the BRP histograms a shorter transfer delay $\Delta_1 = 16$ ms was chosen to achieve similar sensitivity for intra-residue and sequential correlations in HNCA+ and HNCACB+. The main conclusions from these data are the following: (i) Overall, the intra-residue peaks are only very little attenuated in the spectra recorded with the enhanced pulse scheme—less than 10 % for ubiquitin, and less than 15 %

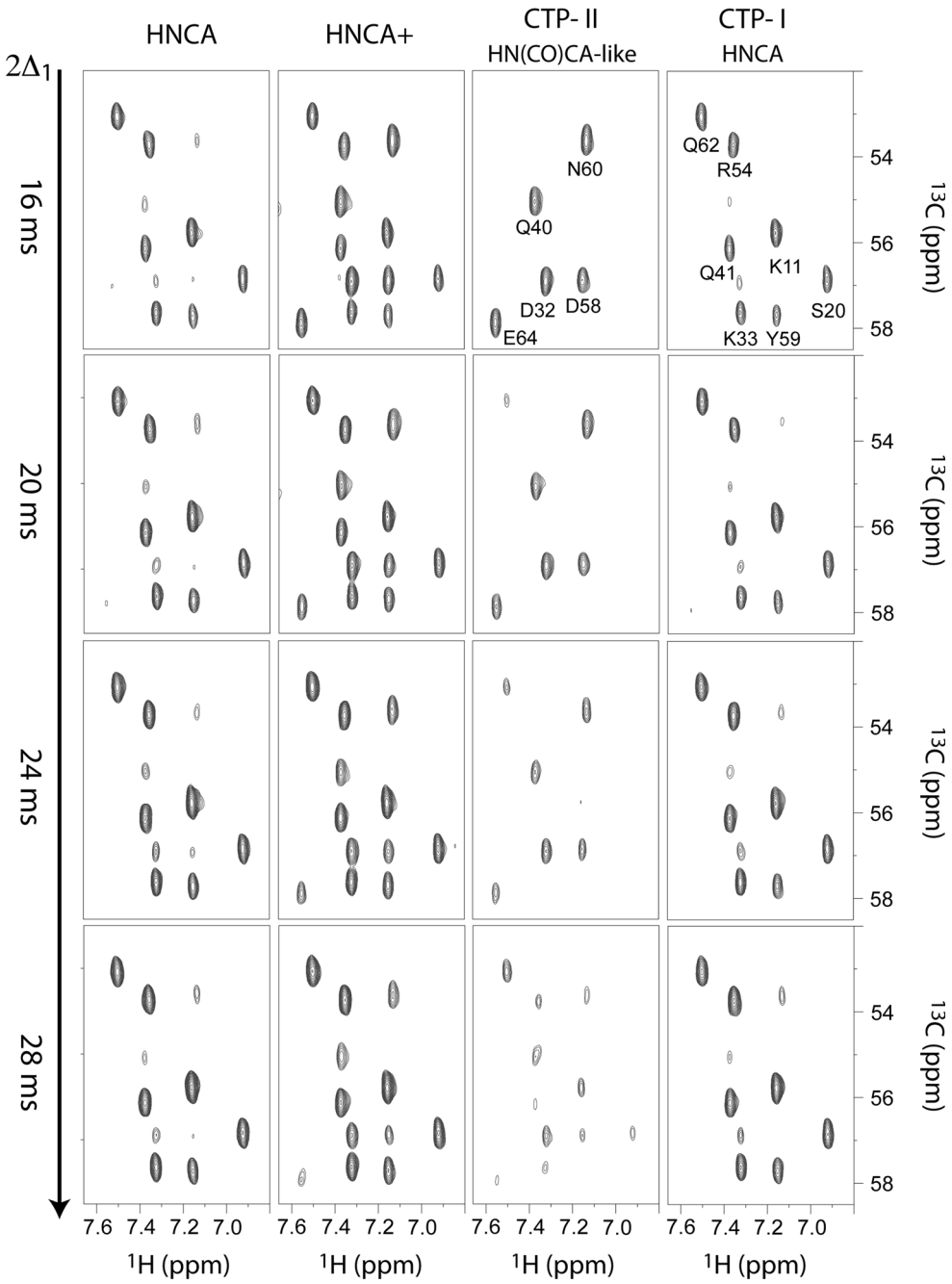

Fig. 3 Experimental comparison of the performance of BT-HNCA and BT-HNCA+ for ubiquitin at 25 °C and 700 MHz. 2D ^{1}H-^{13}C spectra were recorded for $2\Delta_1$ delays (N-CA transfer) varying from 16 to 28 ms. For the enhanced experiment, the complete spectrum (HNCA+), as well as the two subspectra corresponding to CTP-I and CTP-II are shown. The latter are obtained by applying the IPAP-type phase-cycle procedure outlined in Fig. 1. Only a small part of the 2D correlation map is plotted. Annotations refer to the residue type and number of the detected CA frequency. The corresponding plots for HNCO and HNCACB are shown in the Supporting information

for BRP. (ii) The sequential peak intensities are increased by a factor of 2–3 in HNCA+ and HNCACB+, while this sensitivity gain reaches values from 5 to 8 for the HNCO+ experiment. The huge intensity difference observed for sequential correlations in the HNCO+, compared to the HN(CA)CO experiment, is mainly explained by the additional CA → CO transfer step that is only required for CTP-I, and that results in significant additional signal loss for this pathway. (iii) The adjustment of the transfer delay Δ_1 allows to fine-tune the relative intensity of intra-residue and sequential correlation peaks. If a single HNCX+ spectrum is recorded, shortening the delay Δ_1 will enhance the sequential peak with respect to the intra-residue peak intensity. In case the 2 CTPs are separated in different sub-spectra for peak-type (sequential or intra-residue) identification, we recommend the use of short delays Δ_1 in the range 8–10 ms to keep the peak intensity of the minor species in the sub-spectra (sequential peaks in CTP-I, and intra-residue peaks in CTP-II) at a minimum level (see Figs. 3, S1, and S2).

Finally, we have recorded a complete 3D BT-HNCA+ data set for BRP, and 3D BT-HNCACB+ for NS5A. For

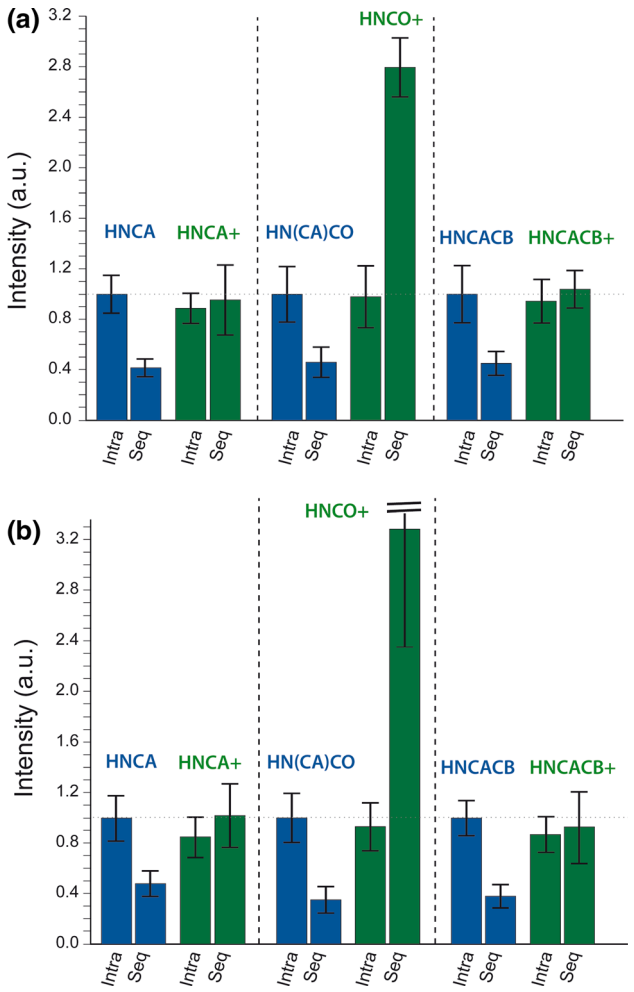

Fig. 4 Intensity histograms (average and standard deviation) of intra-residue and sequential correlation peaks detected in HNCA & HNCA+ (*left*), HN(CA)CO & HNCO+ (*center*), and HNCACB & HNCACB+ (*right*) of **a** ubiquitin (25 °C, 600 MHz, $\tau_C \approx 4$ ns), and **b** BRP (40 °C, 850 MHz, $\tau_C \approx 10$ ns). The N–CA transfer delay was set to $2\Delta_1 = 24$ ms for **a**, and $2\Delta_1 = 16$ ms for **b**. For each experimental pair, intensities were normalized with respect to the average intensity of the intra-residue peaks in the standard experiment. Only residues with well-resolved intra-residue and sequential peaks in the 2D ^{1}H–^{13}C correlation maps were used for this analysis

the latter, we used a sample containing 150 μM [U–^{13}C, U–^{15}N]-labeled NS5A (Non-Structural protein 5A, residues 191–447) from hepatitis C virus in 50 mM potassium phosphate buffer (pH 6.5), 20 mM NaCl, and 2 mM β–mercaptoethanol. The BEST–TROSY implementation allowed for short overall acquisition times of about 12 h per data set, resulting in well resolved, high sensitivity spectra. Strip plots extracted from these 3D data sets are shown in Figs. 5a for BRP and 5b for NS5A. These spectra illustrate the main feature resulting from the enhanced pulse schemes, reported here, the detection of both, intra-residue and sequential correlation peaks of similar intensity throughout the polypeptide sequence. This allows, in favourable cases, to perform sequential resonance assignment from a single 3D data set.

In summary, we have presented herein a set of new triple-resonance pulse schemes for recording H–N–CA, H–N–CO, or H–N–CB correlation spectra of uniformly ^{13}C, ^{15}N-labeled proteins. These HNCA+, HNCO+, and HNCACB+ sequences are easily derived from conventional bi-directional experiments by inserting additional transfer blocks. Compared to their bi-directional counterpart, these pulse sequences yield enhanced sensitivity for sequential correlations, while only slightly attenuating intra-residue peak intensities. In addition, discrimination between sequential and intra-residue correlations is achieved by a simple IPAP-type phase cycle procedure. We have demonstrated the performance of these experiments for BEST–TROSY implementations that reduce signal loss during the additional transfer steps, and allow for high repetition rates, and thus short overall experimental times. Our enhanced pulse sequences present an interesting alternative to conventional assignment experiments in that they ensure the detection of both, sequential and intra-residue correlation peaks in a single experiment, thus potentially reducing the overall experimental time requirements by a factor of 2. In practice, we may distinguish 2 situations where these experiments are of particular advantage. In case of limited sample sensitivity, requiring long experimental times (at least 4 scans per t_1, t_2 increment), our enhanced pulse schemes allow for shared data acquisition, e.g. while recording a HNCA spectrum the complementary HN(CO)CA-like data set is obtained "for free". In case of a limited sample lifetime, the data required for sequential NMR assignment can be recorded twice as fast, or the resolution in the indirect dimensions can be increased for a given experimental time. This may be especially important for NMR studies of IDPs that are often prone to degradation, in-cell studies of proteins (Reckel et al. 2007; Sakakibara et al. 2009; Selenko and Wagner 2007), and real-time NMR investigation of transiently accumulated protein states (Haupt et al. 2011; Rennella et al. 2012), but also for any other protein sample that quickly degrades in the NMR sample tube. For large proteins with short ^{15}N transverse relaxation times the additional CTP-II pathways will no longer significantly contribute to the detected signal. This situation, however, can be improved by deuterating the protein. Although experimentally not demonstrated here, we expect the enhanced TROSY-type HNCX+ pulse schemes to be equally useful for large perdeuterated proteins at high magnetic field strengths.

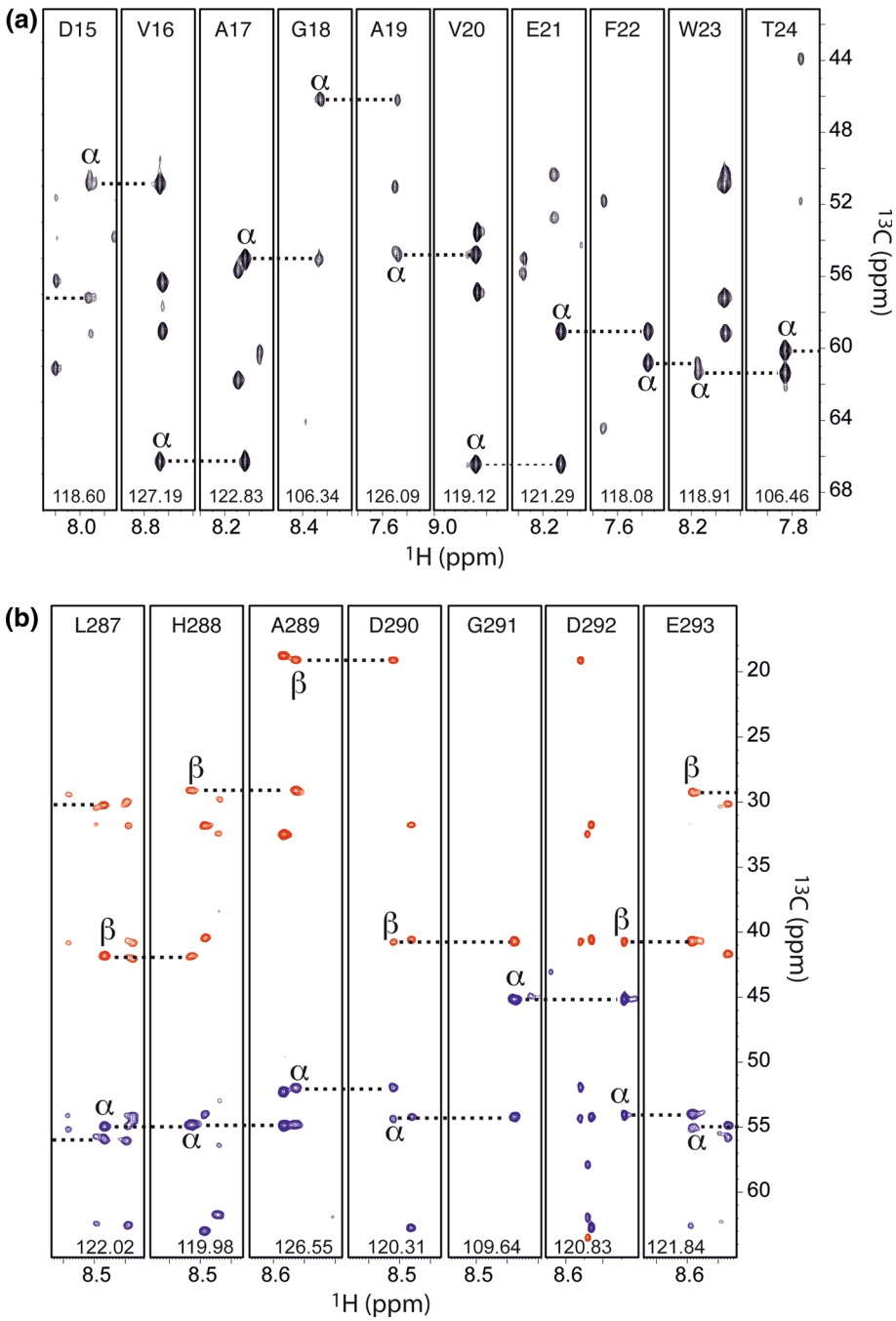

Fig. 5 Strip plots are shown for **a** 3D BT-HNCA+ of the BRP-bleomycine complex (30 kDa, 40 °C, 850 MHz), and **b** 3D BT-HNCACB+ of the intrinsically disordered viral protein NS5A (257 residues, 5 °C, 950 MHz). The 3D HNCA+ spectrum of BRP was recorded with $\Delta_1 = 10$ ms, $\Delta_2 = 15$ ms, $\Delta_3 = 4$ ms, $T_{rec} = 200$ ms, a ^{1}H acquisition time of 71 ms, and 4 scans per (t_1, t_2) increment. In the ^{15}N (^{13}C) dimension, 200 (128) complex points were acquired for a spectral width of 2,757 Hz (6,413 Hz), resulting in a total acquisition time of 12 h. The 3D HNCACB+ spectrum of NS5A was recorded with $\Delta_1 = 11$ ms, $\Delta_2 = 15$ ms, $\Delta_3 = 4$ ms, $\Delta_4 = 3.7$ ms, $T_{rec} = 150$ ms, a ^{1}H acquisition time of 71 ms, and 2 scans per (t_1,t_2) increment. In the ^{15}N (^{13}C) dimension, 300 (200) complex points were acquired for a spectral width of 1,826 Hz (9,815 Hz), resulting in a total acquisition time of 12 h. The sequential assignment walk for the plotted peptide region is shown by *dotted lines*

Acknowledgments We thank Zsofia Solyom for making a sample of NS5A available for this study, and Isabel Ayala for preparation of the ubiquitin sample. This work has been partly supported by grants from the European Union (FP7-I3-BIO-NMR contract No. 261862, FP7-ITN-IDPbyNMR contract No. 264257). S.G. acknowledges support from Bruker Biospin (France). This work used the NMR and isotope labeling platforms of the Grenoble Instruct centre (ISBG; UMS 3518 CNRS-CEA-UJF-EMBL) with support from FRISBI (ANR-10-INSB-05-02) and GRAL (ANR-10-LABX-49-01) within the Grenoble Partnership for Structural Biology (PSB).

References

Boelens R, Burgering M, Fogh RH, Kaptein R (1994) Time-saving methods for heteronuclear multidimensional NMR of (13C, 15 N) doubly labeled proteins. J Biomol NMR 4:201–213

Brutscher B (2002) Intraresidue HNCA and COHNCA experiments for protein backbone resonance assignment. J Magn Reson 156:155–159

Chakraborty S, Paul S, Hosur RV (2012) Simultaneous acquisition of 13Cα–15N and 1H–15N–15N sequential correlations in proteins: application of dual receivers in 3D HNN. J Biomol NMR 52:5–10

Delaglio F, Torchia DA, Bax A (1991) Measurement of 15N–13C J couplings in stahpylococcal nuclease. J Biomol NMR 1:439–446

Farjon J, Boisbouvier J, Schanda P, Pardi A, Simorre JP, Brutscher B (2009) Longitudinal relaxation enhanced NMR experiments for the study of nucleic acids in solution. J Am Chem Soc 131:8571–8577

Favier A, Brutscher B (2011) Recovering lost magnetization: polarization enhancement in biomolecular NMR. J Biomol NMR 49:9–15

Frueh DP, Arthanari H, Wagner G (2005) Unambiguous assignment of NMR protein backbone signals with a time-shared triple-resonance experiment. J Biomol NMR 33:187–196

Geen H, Freeman R (1991) Band-selective radiofrequency pulses. J Magn Reson 93:93–141

Guo C, Zhang D, Tugarinov V (2008) An NMR experiment for simultaneous TROSY-based detection of amide and methyl groups in large proteins. J Am Chem Soc 130:10872–10873

Haasnoot CaG, van de Ven FJM, Hilbers CW (1984) COCONOSY. Combination of 2D correlated and 2D nuclear overhauser enhancement spectroscopy in a single experiment. J Magn Reson 56:343–349

Haupt C, Patzschke R, Weininger U, Groger S, Kovermann M, Balbach J (2011) Transient enzyme À substrate recognition monitored by real-time NMR. J Am Chem Soc 133:11154–11162

Ikura M, Kay LE, Bax A (1990) A novel-approach for sequential assignment of H-1, C-13, and N-15 spectra of larger proteins—heteronuclear triple-resonance 3-dimensional Nmr-spectroscopy—application to calmodulin. Biochemistry 29:4659–4667

Kupce E, Freeman R (1994) Wide-band excitation with polychromatic pulses. J Magn Reson A 108:268–273

Kupče E, Kay LE (2012) Parallel acquisition of multi-dimensional spectra in protein NMR. J Biomol NMR 54:1–7

Kupce E, Boyd J, Campbell ID (1995) Short selective pulses for biochemical applications. J Magn Reson B 106:300–303

Kupče Ē, Kay LE, Freeman R (2010) Detecting the "afterglow" of 13C NMR in proteins using multiple receivers. J Am Chem Soc 132:18008–18011

Nietlispach D, Ito Y, Laue ED (2002) A novel approach for the sequential backbone assignment of larger proteins: selective intra-HNCA and DQ-HNCA. J Am Chem Soc 124:11199–11207

Ottiger M, Delaglio F, Bax A (1998) Measurement of J and dipolar couplings from simplified two-dimensional NMR spectra. J Magn Reson 131:373–378

Permi P (2002) Intraresidual HNCA: an experiment for correlating only intraresidual backbone resonances. J Biomol NMR 23:201–209

Pervushin K, Riek R, Wider G, Wuthrich K (1998) Transverse relaxation-optimized spectroscopy (TROSY) for NMR studies of aromatic spin systems in C-13-labeled proteins. J Am Chem Soc 120:6394–6400

Reckel S, Hänsel R, Löhr F, Dötsch V (2007) In-cell NMR spectroscopy. Prog Nucl Magn Reson Spectrosc 51:91–101

Rennella E, Cutuil T, Schanda P, Ayala I, Forge V, Brutscher B (2012) Real-Time NMR characterization of structure and dynamics in a transiently populated protein folding intermediate. J Am Chem Soc 134:8066–8069

Sakakibara D et al (2009) Protein structure determination in living cells by in-cell NMR spectroscopy. Nature 458:102–105

Salzmann M, Ross A, Czisch M, Wider G (2000) Sensitivity gain by simultaneous acquisition of two coherence pathways: the HNCA(+) experiment. J Magn Reson 143:223–228

Sattler M, Schleucher J, Griesinger C (1999) Heteronuclear multidimensional NMR experiments for the structure determination of proteins in solution employing pulsed field gradients. Prog Nucl Magn Reson Spectrosc 34:93–158

Selenko P, Wagner G (2007) Looking into live cells with in-cell NMR spectroscopy. J Struct Biol 158:244–253

Smith MA, Hu H, Shaka AJ (2001) Improved broadband inversion performance for NMR in liquids. J Magn Reson 151:269–283

Solyom Z, Schwarten M, Geist L, Konrat R, Willbold D, Brutscher B (2013) BEST–TROSY experiments for time-efficient sequential resonance assignment of large disordered proteins. J Biomol NMR 55:311–321

Vanbelle C, Brutscher B, Blackledge M, Muhle-Goll C, Remy MH, Masson JM, Marion D (2003) NMR study of the interaction between Zn(II) ligated bleomycin and Streptoalloteichus hindustanus bleomycin resistance proteins. Biochemistry 42:651–663

Wiedemann C, Bellstedt P, Kirschstein A, Häfner S, Herbst C, Görlach M, Ramachandran R (2014) Sequential protein NMR assignments in the liquid state via sequential data acquisition. J Magn Reson 239:23–28